A Trojan horse transition state analogue generated by MgF_3^- formation in an enzyme active site

Nicola J. Baxter[†], Luis F. Olguin[‡], Marko Goličnik[‡§], Guoqiang Feng[¶], Andrea M. Hounslow[†], Wolfgang Bermel[‖], G. Michael Blackburn[¶], Florian Hollfelder[‡††], Jonathan P. Waltho[†,††], and Nicholas H. Williams[¶††]

[†]Department of Molecular Biology and Biotechnology, University of Sheffield, Sheffield S10 2TN, United Kingdom; [‡]Department of Biochemistry, University of Cambridge, Cambridge CB2 1GA, United Kingdom; [¶]Centre for Chemical Biology, Department of Chemistry, University of Sheffield, Sheffield S3 7HF, United Kingdom; and [‖]Bruker BioSpin GmbH, Silberstreifen 4, 76287 Rheinstetten, Germany

Edited by Perry A. Frey, University of Wisconsin, Madison, WI, and approved July 26, 2006 (received for review May 30, 2006)

Identifying how enzymes stabilize high-energy species along the reaction pathway is central to explaining their enormous rate acceleration. β-Phosphoglucomutase catalyses the isomerization of β-glucose-1-phosphate to β-glucose-6-phosphate and appeared to be unique in its ability to stabilize a high-energy pentacoordinate phosphorane intermediate sufficiently to be directly observable in the enzyme active site. Using ^{19}F-NMR and kinetic analysis, we report that the complex that forms is not the postulated high-energy reaction intermediate, but a deceptively similar transition state analogue in which MgF_3^- mimics the transferring PO_3^- moiety. Here we present a detailed characterization of the metal ion–fluoride complex bound to the enzyme active site in solution, which reveals the molecular mechanism for fluoride inhibition of β-phosphoglucomutase. This NMR methodology has a general application in identifying specific interactions between fluoride complexes and proteins and resolving structural assignments that are indistinguishable by x-ray crystallography.

enzyme mechanism | fluoride inhibition | NMR structure | phosphoryl transfer | isosteric isoelectronic | transition state analogue

Phosphate transfer reactions play a central role in metabolism, regulation, energy housekeeping and signaling (1). As phosphate esters are kinetically extremely stable, efficient catalysis is crucial for the control of these cellular processes. Although model studies have taught us much about the intrinsic chemical mechanisms (2), our understanding of the origins of the enormous enzymatic rate accelerations involved, up to a factor of 10^{21} (3), is far from complete (4). A snapshot of an enzyme in a high-energy state would be immensely useful, as it would allow the very interactions that bring about catalysis to be observed (5). However, is this realistic given how elusive high-energy intermediates and transition states (TSs) inevitably are? The direct observation of TSs for simple organic reactions has required ultrafast lasers with femtosecond resolution (6) and no physical or spectroscopic method is available to observe the structure of TSs of enzymatic reactions directly. Thus transition state analogues that bind tightly in an enzyme active site have been of paramount importance in defining the structural and energetic framework for catalysis (7,8).

An observation that appears to challenge this paradigm arises from structural studies with β-phosphoglucomutase (β-PGM, EC 5.4.2.6): namely, that a high-energy phosphorane on the reaction pathway has been observed directly by x-ray crystallography, demonstrating how the enzyme interacts with a very high-energy, metastable species (9). The latter also apparently demonstrated that the enzyme catalyzed reaction proceeds through an addition–elimination mechanism, a reaction pathway not observed in solution for phosphate monoester anions. However, the observation of an enzyme "caught in the act" is surprising: the demands of turnover mean that the enzyme would gain no apparent advantage in evolving to stabilize such a high energy intermediate to the extent that it is more stable than the enzyme–product complex. The evolutionary driving force for catalysis is to stabilize the transition states for the formation and breakdown of any such intermediate, and very short lifetimes are expected for any high-energy intermediate.

β-PGM is a member of the haloalkanoic dehalogenase superfamily, and catalyses the relocation of a phosphate group on glucose in a ping-pong mechanism as shown in Fig. 1 (10). The physiological substrate β-glucose-1-phosphate (β-G1P) accepts a phosphate group from the phosphoenzyme (β-PGM*) to give the intermediate, β-glucose-1,6-bisphosphate (β-G16BP), which is dephosphorylated to yield the final product, glucose-6-phosphate (G6P). This reaction has an equilibrium constant of 28, which lies in favor of G6P (11). The active site cleft, containing a coordinated magnesium ion cofactor, is formed at the interface of the helical cap domain and the α/β core domain. If β-PGM is crystallized in the presence of β-G1P or G6P a pentacoordinate species can be observed by x-ray analysis, and it is this that has been interpreted as a high-energy metastable intermediate (INT) on the reaction pathway, closely related to the TS (9).

However, this interpretation is not unique. The electron density map is also consistent with a TS analogue (TSA) formed from a five-coordinate magnesium surrounded by two oxygen and three fluoride ligands (MgF_3–TSA) that mimics the phosphoryl group in flight (12, 13). The crystallization buffer needs to contain magnesium and fluoride ions for crystals to form (14, 15), so all of the components necessary for the formation of the MgF_3–TSA are available. Furthermore, *ab initio* quantum-mechanical calculations indicate that MgF_3–TSA is stable, whereas INT is not and spontaneously rearranges to a phosphate monoester covalently bound to either the substrate or the enzyme, as would be expected of a transition state (16). This reassignment would account for the long bond lengths around the central atom (they are typical coordinate bond lengths) and would also remove the requirement that the hitherto unobserved trianionic phosphorane INT be stable for several days at 18°C for crystallization (9, 17). We have probed the identity of the pentacoordinate species by using NMR methodology and kinetic

Author contributions: N.J.B., L.F.O., and M.G. contributed equally to this work; N.J.B., L.F.O., M.G., A.M.H., G.M.B., F.H., J.P.W., and N.H.W. designed research; N.J.B., L.F.O., M.G., A.M.H., W.B., J.P.W., and N.H.W. performed research; G.F. and W.B. contributed new reagents/analytic tools; N.J.B., L.F.O., M.G., F.H., J.P.W., and N.H.W. analyzed data; and N.J.B., L.F.O., M.G., G.M.B., F.H., J.P.W., and N.H.W. wrote the paper.

The authors declare no conflict of interest.

This paper was submitted directly (Track II) to the PNAS office.

Abbreviations: TS, transition state; TSA, TS analogue; β-PGM, β-phosphoglucomutase; β-G1P, β-glucose-1-phosphate; β-G16BP, β-glucose-1,6-bisphosphate; G6P, glucose-6-phosphate; INT, intermediate.

Data deposition: The NMR chemical shifts have been deposited in the BioMagResBank, www.bmrb.wisc.edu (accession nos. 7234 and 7235).

[§]Present address: Institute of Biochemistry, Faculty of Medicine, University of Ljubljana, SI-1000 Ljubljana, Slovenia.

[††]To whom correspondence may be addressed. E-mail: fh111@cam.ac.uk, j.waltho@sheffield.ac.uk, or n.h.williams@sheffield.ac.uk.

www.pnas.org/cgi/doi/10.1073/pnas.0604448103

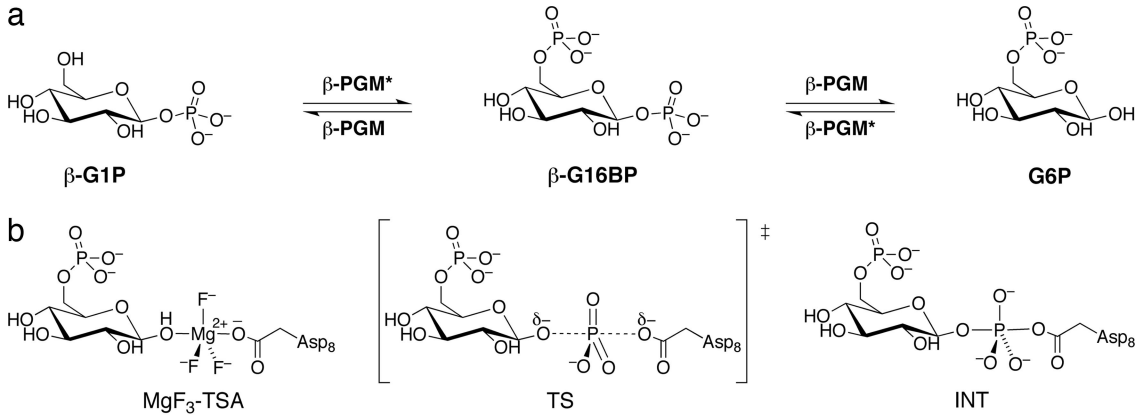

Fig. 1. The reaction mechanism of β-PGM and the potential enzyme stabilized species. (*a*) β-PGM catalyses the interconversion of β-glucose-1-phosphate (β-G1P) and β-glucose-6-phosphate (G6P) via β-glucose-1,6-bisphosphate (β-G16BP) and the phosphorylated form of the enzyme (β-PGM*). (*b*) The TS for the latter part of the β-PGM catalyzed reaction (i.e., β-G16BP to G6P), the proposed phosphorane INT and the TSA (MgF_3–TSA) formed from β-G6P, magnesium, and fluoride.

analysis to establish whether MgF_3^-, which cannot readily be observed in solution, can form in an enzyme active site as an isoelectronic and isosteric mimic of PO_3^-.

Results

We expressed and purified β-PGM according to published procedures (9, 17, 18). Like the related α-PGM enzyme (19), β-PGM had been postulated to be in its phosphorylated form (β-PGM*) when isolated (18), but electrospray mass-spectrometric analysis only shows a peak at 24,207.8 ± 1.8 Da corresponding to the predicted mass of unphosphorylated β-PGM (*Supporting Text* and Fig. 6, which are published as supporting information on the PNAS web site). This is to be expected from the estimated half-life of a carboxyl phosphate ($t_{1/2} \approx 20$ h) for acetylphosphate (20) and is consistent with more recent data on β-PGM (10), but differs from the original report (9). However, β-PGM also exhibits phosphodismutase activity so the enzyme does not need to be initially phosphorylated nor require the addition of the bisphosphorylated intermediate for mutase activity. Phosphorylation of β-PGM by the substrate itself can generate β-PGM* (10) to initiate the catalytic cycle.

Initial NMR experiments confirmed the lack of phosphate in the native enzyme by showing no signal for phosphorus in the ^{31}P NMR spectrum. We then added β-G1P (5 mM) to β-PGM (1 mM) to see whether we could directly detect the proposed phosphorane intermediate using ^{31}P NMR. However, we only observed full turnover of β-G1P (δ ^{31}P 3.00 ppm) into G6P (δ ^{31}P 4.95 and 5.02 ppm for α and β anomers, respectively) within the dead time of the experiment followed by slower hydrolysis over a few hours to leave inorganic phosphate (δ ^{31}P 2.62 ppm) as the final product. Hence, there is no evidence for an accumulation of an enzyme bound phosphorane in solution. On the other hand, in the presence of fluoride and G6P, a new ^{31}P resonance corresponding to a phosphate was observed (δ ^{31}P 5.75 ppm). This signal remained unchanged over at least 2 months, and possessed a 1:1 stoichiometry to the enzyme concentration and a line-width appropriate for an enzyme-bound ligand.

We then used ^{19}F NMR spectroscopy to establish whether the pentacoordinate species could be MgF_3–TSA, i.e., whether fluoride is present in the G6P/β-PGM complex. This approach allows us to distinguish MgF_3^- from the central PO_3^- moiety in INT unambiguously. When β-PGM is added to a solution containing $MgCl_2$ and a 10-fold excess of NH_4F, ^{19}F resonances are observed for free fluoride and for MgF^+ in solution. As soon as either β-G1P or G6P are added, three intense new ^{19}F resonances appear (Fig. 2), each with a 1:1 stoichiometry with the enzyme concentration. When substoichiometric concentrations of fluoride are added into the G6P/β-PGM system, the three ^{19}F resonances appear simultaneously in a 1:1:1 ratio. The appearance of these resonances correlates with a substantial conformational change in the protein, as shown by changes in chemical shift of the backbone amide ^1H and ^{15}N in 2D ^{15}N-TROSY spectra (Fig. 3), corresponding to a transition from an open to a closed conformation (10). NMR resonance assignment of uniformly ^2H,^{13}C,^{15}N-labeled β-PGM both in the open conformation and in the G6P/β-PGM complex was achieved by using methods described in ref. 21. The regions of β-PGM

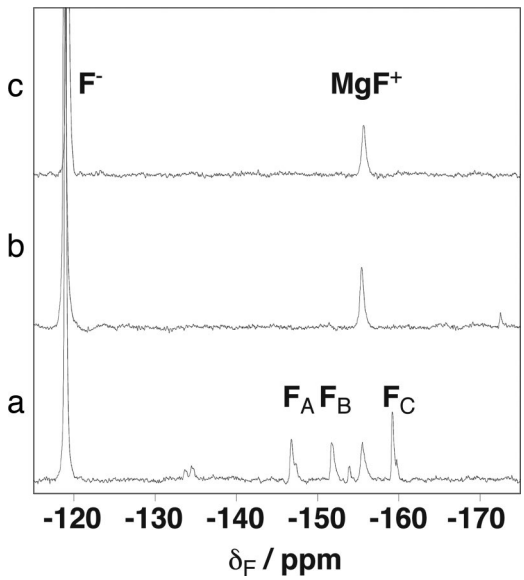

Fig. 2. ^{19}F NMR spectra of the MgF_3^-/β-PGM system. (*a*) The peaks labeled $F_{A\text{-}C}$ (−147, −152, and −159 ppm) correspond to MgF_3^- bound to β-PGM in the presence of G6P. [NH_4F] = 10 mM, [$MgCl_2$] = 5 mM, [β-PGM] = 1 mM, [G6P] = 5 mM. Conditions: pH 7.2, [K^+ Hepes] = 50 mM, 5°C. (*b*) Control with G6P omitted. (*c*) Control with G6P and β-PGM omitted. The peak at −119 ppm is free fluoride in solution (F^-), and the peak at −156 ppm is MgF^+. The three ^{19}F resonances (−134, −135, and −154 ppm), with ≈10% of the intensity of the major peaks, most likely correspond to a minor conformer of the MgF_3–TSA complex that exchanges with the major conformer more rapidly than the complex dissociates, because these resonances correlate via saturation transfer with specific resonances of the major conformer (resonances F_A, F_B, and F_C, respectively).

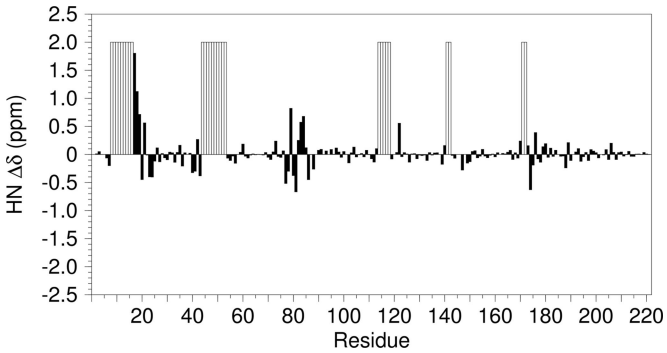

Fig. 3. Histogram of backbone amide proton chemical shift changes ($\Delta\delta$) plotted against residue between β-PGM in the open form and β-PGM in MgF_3–TSA. Positive $\Delta\delta$ represent up-field changes for the open to closed transition. Large $\Delta\delta$ are expected in regions of β-PGM involved in binding substrate in the active site. However, no data were obtained for residues in the active site loops (D8–T16, L44–L53, S114–N118, V141–A142, and S171–Q172) in the open conformation, because the corresponding ^{15}N-TROSY peaks were broadened beyond the limits of detection. This line-broadening behavior is indicative of a conformational dynamics process between two (or more) similarly populated forms, and the difference in ^{1}H chemical shift of $\approx$2 ppm between these interconverting conformations equates to conformational dynamics occurring in the millisecond timescale (i.e., dynamics in the intermediate exchange regime for ^{1}H). These residues are depicted with open bars. Further significant $\Delta\delta$ involve residues A17–Q43 positioned in two α-helices of the ''cap'' domain and N77–S88, which locate to the C-terminal portion of the S65–I84 α-helix and the ''hinge'' region (Q85–Y93). For the remainder of β-PGM, small $\Delta\delta$ indicate that, on formation of MgF_3–TSA, there is little change in the local protein fold outside of these regions.

exhibiting the largest chemical shift changes correspond to those residues which comprise the active site loops, or else residues located in the ''hinge'' region between the ''cap'' and ''core'' domains (10). These NMR observations are consistent with the suggestion that these domains move as rigid bodies relative to each other to enclose the substrate (10).

The new ^{19}F resonances observed indicate that there are three distinct sites for fluoride binding in the G6P/β-PGM complex. Each site is occupied with a lifetime well in excess of 10 s, as determined by the lack of saturation transfer between ^{19}F resonances after selective irradiation of each resonance. The absence of exchange on this time scale with free fluoride in solution and with each other allows these resonances to be used as spectroscopic probes to examine their individual interactions with the protein.

Selective irradiation of each fluoride resonance in turn established the existence of different $\{^{19}F\}^{1}H$-NOE distributions between the three enzyme-bound fluorine nuclei and the protein backbone amide protons. Resolution of the amide proton resonances involved in these NOEs was achieved according to the frequency of their attached ^{15}N nuclei using selective $\{^{19}F\}^{1}H,^{15}N$-HSQC spectra of uniformly $^{2}H,^{15}N$-labeled β-PGM in complex with G6P and fluoride. In total, 11 NOEs were identified between amide protons and the enzyme bound ^{19}F nuclei (Table 1, which is published as supporting information on the PNAS web site). These were used as restraints to move three fluoride ions into the closed conformation of β-PGM (Protein Data Bank ID code 1O08) from random starting coordinates by using standard solution structure determination procedures within the program CNS (22). The resulting positional distribution of fluoride ions (Fig. 4) places them as predicted for the MgF_3–TSA interpretation of the x-ray structural data (9, 12). The new enzyme-bound ^{31}P resonance therefore arises from the phosphate group of G6P when bound to the enzyme (Fig. 4). The combined NMR data show clearly that in the presence of millimolar concentrations of fluoride, the major species present

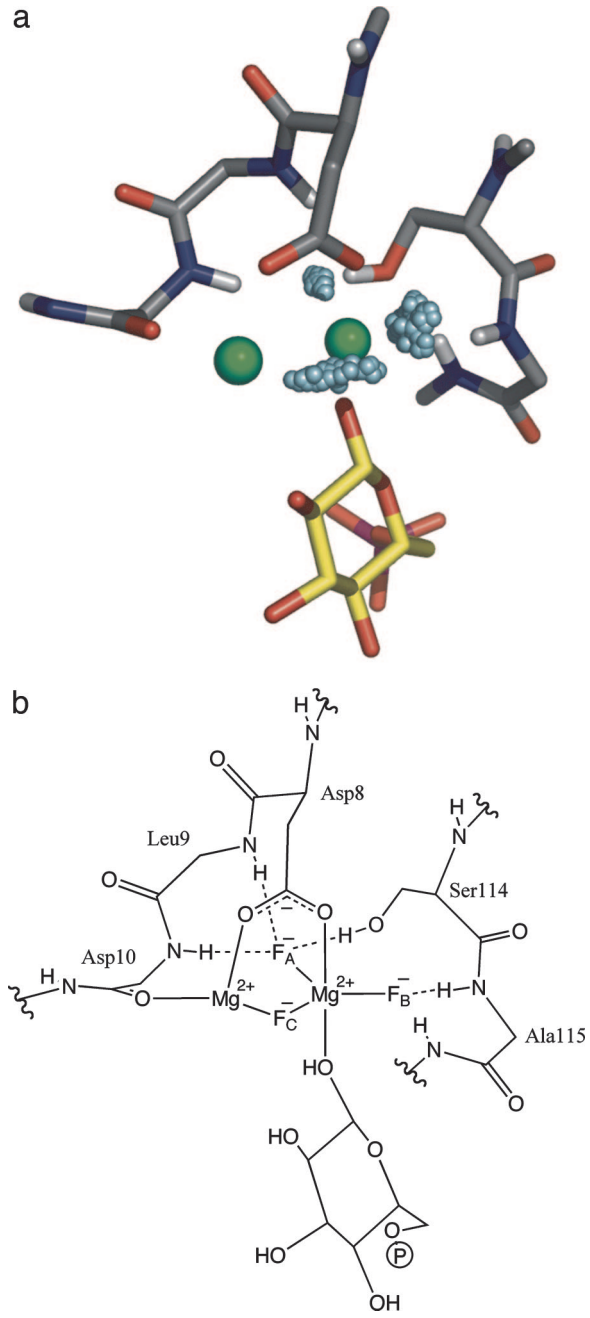

Fig. 4. The structure of the active site in MgF_3–TSA. Positions of fluoride bound to the enzyme were docked according to the 11 NOEs to the backbone amide protons. The protein structure (PDB ID code 1O08) was used as a template, and the fluorides were assigned zero van der Waals radii during their movement so that they could locate the optimum positions in the structure based solely on the NOE restraints. (*a*) The pale blue spheres show the results of 50 separate minimizations. (*b*) The active site of MgF_3–TSA. In *a* and *b*, the magnesium ion essential for catalysis is on the left.

in solution on addition of substrate or product to β-PGM is MgF_3–TSA.

The trigonal-planar MgF_3^- moiety in MgF_3–TSA serves as a mimic for PO_3^-; if this is a good model of the TS, the enzyme should be efficiently inhibited. Fig. 5 shows that under the crystallization (9, 17) and NMR conditions, the reaction is clearly inhibited by fluoride with an apparent K_i in the low mM range. This observation appears to contradict previous reports that β-PGM is not inhibited by added fluoride (14, 15). We note

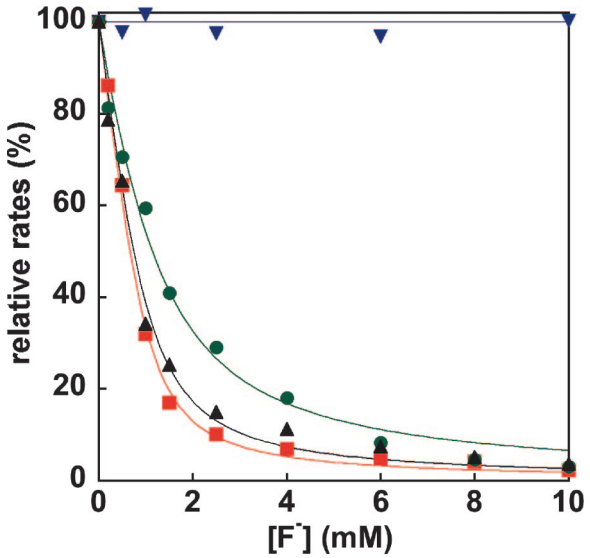

Fig. 5. Fluoride inhibition of catalysis by β-PGM. The reaction is inhibited by fluoride (0–10 mM) unless a high concentration of β-G16BP is present. Relative initial rates (%) are shown for the conversion of β-G1P to G6P. Reactions contained: green circles, [β-G1P] = 250 μM, [β-PGM] = 200 nM; black triangles, [β-G1P] = 250 μM, [α-G16BP] = 50 μM, [β-PGM] = 5 nM; red squares, [β-G1P] = 250 μM, [β-G16BP] = 0.5 μM, [β-PGM] = 5 nM; blue inverted triangles, ([β-G1P] = 50 μM, [β-G16BP] = 200 μM, [β-PGM] = 5 nM.

that kinetic assays of α- and β-PGM are usually run in the presence of either α- or β-G16BP, which accelerate the reaction by saturating the enzyme at the intermediate stage or maintaining its activated, phosphorylated state (10, 15, 19). Only β-G16BP can contribute by maintaining a high concentration of the β-G16BP/β-PGM complex, but other cofactors can stimulate the enzyme by acting as phosphorylating agents, and commercially available α-G16BP is used commonly (10, 23–25). Interestingly α-G16BP is not turned over to G6P by β-PGM, but is converted to α-G1P to generate β-PGM* (10). If the cofactors α- or β-G16BP are used at low concentrations, the enzymatic reaction is still clearly inhibited by fluoride with a similar apparent K_i (Fig. 5). However, the published inhibition study was conducted under the unusual conditions of a 2-fold excess of intermediate β-G16BP (200 μM) to substrate β-G1P (100 μM) (15). When we repeated our experiments in the presence of high concentrations of β-G16BP, we also observed that even 10 mM fluoride did not inhibit the reaction (Fig. 5). Under these conditions, pre-steady-state kinetics with β-PGM and β-G16BP show a burst of product G6P release followed by steady-state hydrolysis of phosphoenzyme (data not shown), which indicates that high concentrations of β-G16BP maintain β-PGM in a phosphorylated state. With the enzyme phosphorylated on the nucleophilic aspartate, MgF_3–TSA simply cannot form.

Discussion

All of the structural and kinetic observations described above, and the previous x-ray data, are consistent with the formation of MgF_3–TSA when G6P, magnesium, and fluoride are present with β-PGM. Reassigning the pentacoordinate species as a transition state analogue necessarily limits the inferences that can be drawn from the structure as the bond lengths and electrostatic contacts will be governed by the intrinsic ground state properties of the analogue, and thus do not necessarily reflect the bond lengths in the TS or potential INT. However, the central MgF_3^- moiety is both isoelectronic and isosteric with metaphosphate PO_3^- and so provides a closer portrayal of the expanded TS for phosphate monoester transfer in solution than aluminum and beryllium fluoride complexes which have been more widely utilized to date (13, 26–28). The intrinsic binding constant of MgF_3^- to the enzyme-substrate complex will be considerably lower than the observed K_i as MgF_3^- has a very low formation constant in aqueous solution [MgF^+ has log $\beta_1 = 1.7$ and MgF_2 has log $\beta_2 \leq 3.2$ (29); MgF_3^- has not been observed in solution], which means that it is only observable in the enzyme active site. This low solution stability suggests that magnesium trifluoride will be a sensitive probe for identifying active sites that strongly stabilize such trigonal–bipyramidal species with a similar charge distribution, because productive interactions with the enzyme pocket are required for assembly of the transition state analogue. Consistent with this expectation, the simultaneous appearance of the fluoride resonances in the same ratio as the final complex together with a concomitant transition of β-PGM from the open to closed conformation on titration of the G6P/β-PGM system with fluoride is conclusive evidence that MgF_3–TSA assembles cooperatively and is stoichiometric with β-PGM concentration.

These observations have broad implications for understanding the basis of and potential for fluoride inhibition of enzymes that catalyze phosphoryl transfer in the presence of magnesium ions. Fluoride inhibition of certain enzymes has been linked to its mammalian toxicity and to its therapeutic action in dental health. The growth of *Treponema*, *Actinomyces*, *Fusobacterium*, and *Bacteroides* species is inhibited by millimolar concentrations of fluoride and this has been linked to fluoride inhibition of acid and alkaline phosphatases (30). The proton translocating enzyme F_oATPases of oral bacteria are also inhibited by fluoride at millimolar concentration (31). In general, such fluoride inhibition has been attributed to the replacement of an essential water or hydroxide ion in the active complex by fluoride (32), but it is likely that formation of MgF_3^- in the active site may be the true inhibitor in some cases; and it may be particularly important in affecting the most proficient enzymes which have exceptionally strong formal transition state affinities (3, 7).

Here, we present a detailed characterization of a metal ion–fluoride complex bound to an enzyme active site in solution, and reveal the molecular mechanism for fluoride inhibition of β-PGM. These results show that it is possible for fluoride ions to be located in an enzyme–analogue complex in solution with high structural accuracy. Hence, MgF_3–TSA has the potential to allow us to define the solution structure of the active site as it is arranged around a mimic for the transferring phosphoryl moiety. The high susceptibility of ^{19}F NMR chemical shifts to the local electronic environment provides a sensitive probe of subtle changes within the enzyme that would be invisible to other structural biology methods. These methods can also be applied to the study of other complexes that contain metal–fluoride species as analogues for phosphates, such as aluminum (27, 33) and beryllium (26, 34) fluorides, and will enable the accurate assignment of their identity in future. The potential utility of using fluoride as a probe of enzyme structure is especially powerful when used in combination with an electronically and geometrically accurate transition state mimic for phosphoryl transfer, MgF_3^-, that only exists within the confines of the active site and places the spectroscopically active atoms right into the catalytic cavity.

Materials and Methods

Expression and Purification of β-PGM. The β-PGM gene was amplified from a *Lactococcus lactis* strain obtained from DSMZ (Braunschweig, Germany) (no. 20481, which is identical to ATCC strain 19435). This strain was grown at 30°C on plates with corynebacterium agar containing casein peptone tryptic digest (10 g), yeast extract (5 g), glucose (5 g), NaCl (5 g), agar (15 g), and distilled water (1,000 ml) adjusted to pH 7.2–7.4. A toothpick-scrape of a colony was used as a template in a PCR to

amplify the gene. Primers (5′-GAA TTC CAT ATG TTT AAA GCA GTA TTG-3′ and 5′-CCG CTC GAG TTA TTT TTG CTT TTG AAG-3′) were used to introduce a NdeI and a XhoI restriction site at the beginning and end of the gene, respectively. After digestion, the PCR product was cloned in the pET-22b(+) expression vector (Novagen, San Diego, CA) giving the expected published sequence (35). Transformed *Escherichia coli* BL21(DE3) with this plasmid were used to overexpress β-PGM. The expression and purification of the protein were carried out exactly as described in ref. 17.

Expression and Purification of Labeled β-PGM. For ^{15}N-, $^{15}N/^{2}H$-, and $^{15}N/^{13}C/^{2}H$-labeled protein samples, cells were grown in minimal M9 media as described in ref. 21 except that $^{15}NH_4Cl$ was used in all three samples; glucose was the carbon source for the ^{15}N-labeled protein, and 1 mM IPTG was used to induce expression. The purification procedure followed was the same as for unlabelled β-PGM (17).

NMR Methods. The samples prepared for the NMR analysis of MgF_3–TSA contained: 1 mM β-PGM, 5 mM β-G1P or G6P, 5 mM $MgCl_2$, and 10 mM NH_4F in 50 mM K^+ Hepes buffer (pH 7.2) containing 15% vol/vol D_2O, 2 mM NaN_3, and EDTA-free Complete protease inhibitor mixture. The 1D ^{19}F NMR spectra were recorded at 5°C on a Bruker Avance 500 MHz spectrometer (operating at 470.59 MHz for fluorine) equipped with a 5-mm dual $^{1}H/^{19}F$ probe. The 2D frequency selective $\{^{19}F\}^{1}H,^{15}N$-HSQC NOE difference spectra of $^{2}H,^{15}N$-labeled β-PGM in MgF_3–TSA (sample prepared as above except with 20 mM G6P) were acquired at 25°C on a Bruker Avance 600 MHz spectrometer (operating at 564.69 MHz for fluorine) equipped with a $^{1}H/^{15}N/^{19}F$ probe and *z* axis gradients. Selective ^{19}F irradiation was achieved with a continuous wave at a power level of 40 dB applied over the 1-s recycle delay and the solvent signal was minimized with water flip-back pulses. The spectra were acquired as four interleaved $^{1}H,^{15}N$-HSQC experiments with defined selective irradiation frequencies of −147, −152, and −159 ppm and one at an off-resonance position. Three 2D frequency selective $\{^{19}F\}^{1}H,^{15}N$-HSQC spectra were obtained by subtracting the spectra recorded with defined ^{19}F irradiation frequencies from the off-resonance spectrum. For the backbone resonance assignment of β-PGM in MgF_3–TSA, NMR spectra were acquired at 25°C on a sample of $^{2}H,^{15}N,^{13}C$-labeled β-PGM (sample prepared as above except with 20 mM G6P) using a Bruker Avance 600 MHz spectrometer equipped with a 5-mm $^{1}H/^{15}N/^{13}C/^{2}H$ cryoprobe and pulse-field z-gradients. Backbone resonance assignments for HN, N, C^{α}, C^{β}, and C′ nuclei were obtained from 2D ^{15}N-TROSY, 3D TROSY ct-HNCA, 3D TROSY ct-HN(CO)CA, 3D TROSY HN(CA)CB, 3D TROSY HN(COCA)CB, 3D TROSY HN(CA)CO, and 3D TROSY HNCO. The data were acquired, processed, and analyzed and backbone sequential assignment was performed as in ref. 21. Backbone sequential assignment of β-PGM in the open conformation was performed as for β-PGM in MgF_3–TSA using a sample containing 1 mM β-PGM, 5 mM $MgCl_2$, and 10 mM NH_4F in 50 mM K^+ Hepes buffer (pH 7.2) with 15% vol/vol D_2O, 2 mM NaN_3, and EDTA-free Complete protease inhibitor mixture. Proton chemical shifts were referenced relative to the methyl signals of internal DSS at 0.0 ppm. ^{15}N, ^{13}C, and ^{19}F chemical shifts were calculated indirectly by using the following gyromagnetic ratios: $^{15}N/^{1}H = 0.101329118$, $^{13}C/^{1}H = 0.251449530$, and $^{19}F/^{1}H = 0.940940080$. The backbone ^{1}H, ^{13}C, and ^{15}N chemical shifts for β-PGM in both the MgF_3–TSA complex and in the open conformation together with the three ^{19}F chemical shifts of the MgF_3^- species have been deposited in the BioMagResBank under accession codes 7234 (MgF_3–TSA complex) and 7235 (open conformation).

β-PGM Kinetic Assays. All β-PGM assays were carried out in a Molecular Devices (Sunnyvale, CA) Microtitreplate Spectramax Plus Reader at 25°C in 50 mM K^+ Hepes (pH 7.2) with 100 μl total volume containing 2 mM $MgCl_2$ and 5 nM β-PGM unless stated otherwise. All substrates were obtained commercially from Fluka (St. Louis, MO) and Sigma (St. Louis, MO) except for β-G16BP which was synthesized from α-D-glucose (Scheme 1, which is published as supporting information on the PNAS web site). Enzyme concentrations were measured by using $\varepsilon_{280} = 20.6\ \mu M^{-1}\cdot cm^{-1}$ determined by the Biuret method (36) with commercial BSA standards (Sigma) used for the calibration. The appearance of G6P was monitored in a coupled assay with glucose-6-phosphate dehydrogenase (obtained from Sigma, 5 units/ml G6PDH and 0.5 mM NAD^+) following the absorbance at 340 nm. Reactions were initiated by the addition of the substrate. The steady-state rates were calculated from the linear portions of time courses and when less than 20% of substrate was converted. Fluoride inhibition of glucose-6-phosphate dehydrogenase could not be detected below 100 mM in our experimental setup. Any inhibitory effects can therefore be ascribed to effects on β-PGM alone.

We thank Steve Gamblin and Steve Smerdon for helpful discussion and Tony Kirby for helpful comments on the manuscript. M.G. is a European Union Marie Curie fellow, and L.F.O. holds a Consejo Nacional de Ciencia y Tecnología (Mexico) predoctoral fellowship. This research was supported by the European Union network ENDIRPRO, the Biotechnology and Biological Sciences Research Council, and the Medical Research Council.

1. Dzeja PP, Terzic A (2003) *J Exp Biol* 206:2039–2047.
2. Schramm VL (1998) *Annu Rev Biochem* 67:693–720.
3. Lad C, Williams NH, Wolfenden R (2003) *Proc Natl Acad Sci USA* 100:5607–5610.
4. Benkovic SJ, Hammes-Schiffer S (2003) *Science* 301:1196–1202.
5. Knowles J (2003) *Science* 299:2002–2003.
6. Zewail AH (2000) *Angew Chem Int Ed Engl* 39:2586–2631.
7. Wolfenden R (2003) *Biophys Chem* 105:559–572.
8. Schramm VL (2005) *Curr Opin Struct Biol* 15:604–613.
9. Lahiri SD, Zhang G, Dunaway-Mariano D, Allen KN (2003) *Science* 299:2067–2071.
10. Zhang G, Dai J, Wang L, Dunaway-Mariano D, Tremblay LW, Allen KN (2005) *Biochemistry* 44:9404–9416.
11. Marechal LR, Belocopitow E (1974) *Eur J Biochem* 42:45–50.
12. Blackburn GM, Williams NH, Gamblin SJ, Smerdon SJ (2003) *Science* 301:1184c.
13. Graham DL, Lowe PN, Grime GW, Marsh M, Rittinger K, Smerdon SJ, Gamblin SJ, Eccleston JF (2002) *Chem Biol* 9:375–381.
14. Allen KN, Dunaway-Mariano D (2003) *Science* 301:1184d.
15. Tremblay LW, Zhang G, Dai J, Dunaway-Mariano D, Allen KN (2005) *J Am Chem Soc* 127:5298–5299.
16. Webster CE (2004) *J Am Chem Soc* 126:6840–6841.
17. Lahiri SD, Zhang G, Radstrom P, Dunaway-Mariano D, Allen KN (2002) *Acta Crystallogr D* 58:324–326.
18. Lahiri SD, Zhang G, Dunaway-Mariano D, Allen KN (2002) *Biochemistry* 41:8351–8359.
19. Ray WJ, Peck EJ (1972) *Enzymes* 6:407–477.
20. Di Sabato G, Jencks WP (1961) *J Am Chem Soc* 83:4393–4400.
21. Reed MAC, Hounslow AM, Sze KH, Barsukov IG, Hosszu LLP, Clarke AR, Craven CJ, Waltho JP (2003) *J Mol Biol* 303:1189–1201.
22. Brunger AT, Adams PD, Clore GM, Delano WL, Gros P, Grosse-Kunstleve RW, Jiang J-S, Kuszewski J, Nilges M, Pannu NS, *et al.* (1998) *Acta Crystallogr D* 54:905–921.
23. Qian NY, Stanley GA, Hahn-Hagerdal B, Radstrom P (1994) *J Bacteriol* 176:5304–5311.
24. Mesak LR, Dahl MK (2000) *Arch Microbiol* 174:256–264.
25. Lahiri SD, Zhang G, Dai J, Dunaway-Mariano D, Allen KN (2004) *Biochemistry* 43:2812–2820.
26. Kagawa R, Montgomery MG, Braig K, Leslie AG, Walker JE (2004) *EMBO J* 23:2734–2744.
27. Yu YW, Morera S, Janin J, Cherfils J (1997) *Proc Natl Acad Sci USA* 94:3579–3583.

28. Grigorenko BL, Nemukhin AV, Cachau RE, Topol IA, Burt SK (2005) *J Mol Model* 11:503–508.
29. Fovet Y, Gal JY (2000) *Talanta* 53:617–626.
30. Li L (2003) *Crit Rev Oral Biol Med* 14:100.
31. Ahmad Z, Senior AE (2006) *FEBS Lett* 580:517–520.
32. Lebioda L, Zhang E, Lewinski K, Brewer JM (1993) *Proteins: Struct Funct Genet* 16:219.
33. Schlichting I, Reinstein J (1999) *Nat Struct Biol* 6:721–723.
34. Cho H, Wang W, Kim R, Yokota H, Damo S, Kim SH, Wemmer D, Kustu S, Yan D (2001) *Proc Natl Acad Sci USA* 98:8525–8530.
35. Qian N, Stanley GA, Bunete A, Radstrom P (1997) *Microbiology* 143: 855–865.
36. Lowe CR, Thomas JA (1996) in *LabFax Enzymology*, ed Engel PC (Academic, New York), pp 34–40.